Conversion of foliar residues of the ornamental species Sansevieria trifasciata into adsorbents: the study of dye adsorption in continuous and discontinuous systems

Patrícia Grassi
Federal University of Santa Maria
Matias Schadeck Netto
Federal University of Santa Maria
Sérgio Luiz Jahn
Federal University of Santa Maria
Jordana Georgin
Federal University of Santa Maria, UFSM
Dison S.P. Franco
Universidad de la Costa, CUC
Mika Sillanpää
University of Johannesburg
Lucas Meili (lucas.meili@ctec.ufal.br)
Federal University of Alagoas
Luis F. O. Silva
Universidad de la Costa, CUC

Research Article

Keywords: leaf powder, continuous, discontinuous, adsorption, methylene blue

Posted Date: April 12th, 2022

DOI: https://doi.org/10.21203/rs.3.rs-1534621/v1

Abstract

The species *Sansevieria trifasciata* is very widespread around the world both for its ornamental use and profusely spread among religions of African origin. The study analyzed the potential of leaf powder prepared from the residual leaves of the species *Sansevieria trifasciata*, as a potential adsorbent for methylene blue (MB) removal in a discontinuous system. For the batch study, the equilibrium was reached fast for almost all concentrations after 60 min, obtaining the maximum capacity of 139.98 $mg.g^{-1}$ for 200 $mg.L^{-1}$. The increase in temperature disfavored the dye adsorption, with the maximum adsorption capacity of 225.8 $mg.g^{-1}$, observed for 298 K. The thermodynamic parameters confirmed that the adsorption process is spontaneous and exothermic. A direct sloping curve was established for the fixed bed, with breakthrough time (t_b) of 1430, 1130, and 525 min for 100, 200, and 500 $mg.L^{-1}$, respectively. The column stoichiometric capacities (q_{eq}) and the mass transfer zone lengths (Z_m) were 60.48, 187.01, 322.65 $mg.g^{-1,}$ and 8.81, 11.28 and 10.71 cm, for concentrations of 100, 200, and 500 $mg.L^{-1}$, correspondingly. Furthermore, in a mixture of several dyes, the adsorbent obtained the removal of 51% of the color.

1. Introduction

Synthetic dyes are widely applied in different industries such as cosmetics, pharmaceuticals, textiles, printing, and food [1]. The textile industry generates approximately 54% of the total dye effluent [2]. Most dyes are toxic, carcinogenic, and teratogenic pollutants due to their high water solubility and low biodegradability [3]. They are to blame for the prevalence of color in textile wastewater, which obstructs light penetration and endangers aquatic habitats. Highly colored wastewaters interfere with the passage of solar radiation through water, disrupting aquatic ecosystems [4–6]. However, to protect human health and the environment, it is necessary to remove these contaminants from wastewater [7, 8].

Adsorption is a simple operation that relies on the availability of a large range of adsorbents, making it a viable approach for reducing dissolved dye concentrations in industrial effluents. The dyes contained in an aqueous effluent are transferred to a solid phase via adsorption, dramatically reducing the dyes' bioavailability. The adsorbent can then be renewed or kept in a dry area away from the environment, and the decontaminated effluent can be discharged back into the environment [9–14]. In this context, we can say that the application of adsorbents in batch systems is well documented in the literature, thus the application in continuous adsorption should be prioritized. Although, fixed bed operations are little explored on a laboratory scale. Evidently, fixed bed operation can be used for commercial expansion of water treatment processes [15].

There are numerous studies in the literature aiming on the phenomenological examination of the key process factors influence. However, due to the widespread use of adsorption technology, researchers are still interested in finding novel and unexploited sources for adsorbent materials, adjustment operating parameters for low-cost synthesis, and effective uptake of certain pollutants [16, 17]. In recent years, many adsorbents obtained from natural materials such as clay minerals [18], agricultural residues, and

by-products such as coffee residues [19], sugarcane bagasse [20, 21], soybean hulls [22], rice [23], peanuts [24, 25], tree bark [26–28], coconut [29], and industrial waste such as graphene oxide [30] and fly ash [31], were applied for the removal of dyes from the aqueous solution. Among the studied, leaf-based materials (crude or activated forms) have received greater attention, mainly because they are inexpensive, available in large quantities in almost all regions of the world, require only a few preparation steps and, in many cases, have no other application [32].

The species *Sansevieria trifasciata*, popularly known as the Saint George's sword is a succulent belonging to the Ruscaceae family. It has long, erect leaves and a rigid structure. They are ornamental plants and known to be air purifiers, as they absorb various organic chemicals such as xylene, toluene, and formaldehyde and can withstand various environmental conditions [33]. *Sansevieria trifasciata* is also used for the treatment of inflammation and sold in natura in the market to treat snakebites and in the treatment of earaches, swelling, boils, and fever [34]. Functional groups present in the leaves, such as carboxyl, amine, and hydroxyl, serve as binding sites in the adsorption process, making these adsorbents effective [32, 33].

The study analyzed the potential of powder prepared from the residual leaves of the species *Sansevieria trifasciata*, as a potential low-cost adsorbent in the removal of methylene blue (MB) dye in a discontinuous system. Aiming at further application in industrial fixed-bed systems, the adsorbent was also analyzed in a pilot column. The leaf powder was characterized by different characterization techniques. Optimal dosage and pH experiments were first conducted. Adsorption kinetics were evaluated for different initial concentrations of the adsorbate. The equilibrium studies were investigated varying the temperature from 298 to 328 K. Finally, the thermodynamic parameters of adsorption were estimated. The efficiency of the adsorbent to treat a synthetic mixture containing several dyes and salts was analyzed.

2. Materials And Methods

2.1 Materials and characterization

The leaves of the species *Sansevieria trifasciata* were obtained from a flower shop, where part of the biomass, due to its color and older appearance, is often discarded. The residual material was washed with distilled water. Then the leaves were dried in an oven for 24 h at a temperature of 333.15 K. The dried samples were crushed with the aid of a knife mill and then passed through 100 µm sieves. The samples were separated to be further characterized and the remains were employed in the adsorption experiments.

The adsorbent was characterized by Fourier Transform Infrared Spectroscopy (FTIR) in a spectrophotometer (Perkin Elmer, USA) in the range of 4000 – 400 cm^{-1}. The X-Ray Diffraction (XRD) measurements were conducted on a diffractometer (Rigaku Miniflex model 300) applying Cu-Kα radiation (λ = 1.5418 Â). Morphology was evaluated through scanning electron microscopy (Tescan-Vegan 3 equipment).

2.2 Adsorption experiments

All batch adsorption experiments were conducted in triplicate, using a thermostatic stirrer (Marconi, MA 093, Brazil) at 150 rpm. The influence of adsorbent dosage on contaminant removal was assessed in 50 mL of solutions for concentration 100 $mg.L^{-1}$ at pH 7, varying the dosage by 0.5; 0.75; 1.0; 1.25 and 1.5 $g.L^{-1}$, at a temperature of 298 K for 120 min. The effect of pH was evaluated with 50 mL of solutions at 100 $mg.L^{-1}$, varying the pH values from 2 to 10, using the dosage previously defined, at 298 K for 120 min. The pH values were determined measured using a pHmeter (Digimed, DM 20, Brazil) and adjusted with 0.1 N of HCl and 0.1 N of NaOH solutions.

To determine how the contact time can affect the dye adsorption, the kinetics were performed at initial concentrations of 50, 100, 150, and 200 $mg.L^{-1}$, the best pH and adsorbent dosage previously defined, at 298 K until the equilibrium. The isotherms were assessed stirring 50 mL of MB solutions and ranging the initial concentrations from 50 to 500 $mg.L^{-1}$ at 298, 308, 318, and 328 K. The solutions concentration was measured using a spectrometer (Biospectro SP-22, Brazil) at 664 nm. The adsorption capacities at the specified time (q_t, $mg.g^{-1}$), at the equilibrium (q_e, $mg.g^{-1}$), and the removal efficiency (R, %), were determined according to the equations presented in the Supplementary Material **S.1**

2.3 Kinetic models, Isotherm models, and estimation of thermodynamic parameters

The adsorption operation was evaluated according to well-documented procedures in terms of kinetics [35–37], isotherms [38–40], and thermodynamics [41]. All information is presented in Supplementary Material **S2** through **S4**.

2.4 Evaluation of simulated Textile Effluent adsorption

An effluent was produced to evaluate the leaf powder applicability under real conditions. Thus, the solution was produced to simulate the industrial textile effluents. The composition of simulated effluent is shown in Table S1. The studies were conducted at 298 K, and at the original solution pH, using 0.8 $g.L^{-1}$ of adsorbent dosage. The tests were executed using the best parameters previously obtained. Spectra of treated and untreated effluents were acquired using a UV-Vis spectrophotometer (Shimadzu, UV-2600, Japan) at 300 to 800 nm. The dye removal was achieved as a relation of the areas under the spectral curves.

2.5 Fixed bed adsorption experiments and model fitting

Continous adsorption tests were conducted to further explore the application of the *Sansevieria trifasciata* powder. For this, an apparatus equipped with a reservoir, a peristaltic pump (Provitec, model AWV, Brazil, maximum flow rate of 1.2 $L.h^{-1}$), and a fixed bed (acrylic column 25 cm length and 2.5 cm diameter). The experiments were executed changing the inlet MB concentration (100, 250, and 500 $mg.L^{-1}$), with a flow rate of 0.9 $L.h^{-1}$ and a fixed bed height of 25 cm, corresponding to an adsorbent mass of

35.6 g. The measurement of the outlet MB concentration was determined through an UV-Vis spectrophotometer (Shimadzu, model UV min 1240, Japan). The estimation of the stoichiometric adsorption capacity (q_{eq} $mg.g^{-1}$), the percentage of removal, and mass transfer zone length (Z_m, cm) were determined according to equations 1 and 2.

$$q_{eq}=\frac{QC_0}{m_{ads}}\int_0^{t_{total}}\left(1-\left(\frac{C_t}{C_0}\right)\right)dt \quad (1)$$

$$Z_m=L\left(1-\frac{t_b}{t_e}\right) \quad (2)$$

where q_{eq} is the maximum adsorption capacity of the column ($mg.g^{-1}$), C_0 is the initial concentration ($mg.L^{-1}$), t_{total} is the total experiment time (min), Q is the volumetric flow ($mL.min^{-1}$), L is the fixed bed heigh column (cm), m_{ads} is the adsorbent mass (g), t_b is the breakthrough time (min) when C_t/C_0 is 0.05, t_e is exhaustion time when the C_t/C_0 is 0.95. The Thomas [42] and Yoon-Nelson models, presented in Supplementary Material **S6**, were selected as dynamic models.

2.6 Parameters estimation and statistical evaluation

The initial guess and estimation of the parameters of kinetic, isotherm, and dynamic models were conducted through Matlab scripting. For this, the following built-in function where employed: the *particleswarm* was employed for the initial guess for all models, with a swarm size of 50. After that the initial guess were employed in the *lsqnonlin* for models with parameters restriction and *nlinfit* for the model without parametric restriction. The *lsqnonlin* and the *nlinfit* employes the minimum least squared as the objective function. Last, statistical indicators (determination coefficient (R^2), adjusted determination coefficient (R^2_{adj}), average relative error (ARE), mean squared error (MSR)), the equations are displayed in the Supplementary Material, were used to evaluate the models fitting.

3 Results And Discussions

3.1 Characteristics of adsorbent

In Fig. 1(I) the X-ray diffraction spectrum is visible where the presence of broadband between 15 and 400 is observed, which indicates that no mineral phase is present. Therefore, the leaf powder has a highly amorphous structure. The amorphous phase is characterized by the broad peak that can be attributed to the lignin content [43]. Similar XRD patterns were also observed by other authors using structures of materials of natura plant origin [26, 44, 45].

In the FT-IR spectrophotometer of the leaf powder, several functional groups present on the surface of the adsorbent were observed. As can be seen in Fig. 1(II), the strong band at 3442 cm^{-1} can be attributed to the vibrations of the hydroxyl group attached to the cellulose and lignin molecules or to the adsorbed

water [32]. The bands at 2922 cm^{-1} belong to the asymmetric C-H elongation of alkyl groups [46]. Bands at 1627 cm^{-1} indicate C-O elongation of the carbonyl group [2]. The vibration frequencies in the region 1338 – 1058 cm^{-1} represent the elongation of C-O belonging to alcohol, phenol, ethers, and carboxylic acid groups [33]. These findings suggest that the leaf powder contains a number of functional groups that are typical to lignocellulosic materials, which exhibit ion exchange capacity and general sorption properties derived from their polymeric components and structure. These polymers have sorption properties for a wide variety of metallic solutes and cations.

The surface micrograph of the material under different magnifications is shown in Fig. 1(III). In general, the samples have a morphology that consists of a smooth and fibrillar structure, without a defined geometry. In Figs. 1(III), C and D, the occurrence of cavities and pores that are favorable to adsorption, as they allow the penetration of dyes in the adsorbent structure can be observed. In the literature, it is common to find this type of morphology in plant materials in natural form [27, 47, 48].

3.2 Effects adsorbent dosage on removal of methylene blue

The effect of adsorbent dosage was studied ranging from 0.5 to 1.5 $g.L^{-1}$ (Fig. 2a). The first point to be analyzed is that increasing the dosage from 0.5 to 1.5 $g.L^{-1}$ caused a decrease in the adsorption capacity (q_t) from 129.66 to 58.31 $mg.g^{-1}$. This is because, at higher doses, the adsorption sites aggregate, and the adsorbent is not fully utilized. Mathematically, this tendency can be easily explained by Eq. (1) [49]. Furthermore, the MB removal efficiency increased from 62.26 to 83.87% with increasing dosage, which can be attributed to the greater number of adsorption sites for MB [50]. Therefore, 0.8 $g.L^{-1}$ of foliar powder was selected as the optimal dosage, this being the intersection point of the curves in the graph.

3.3. pH effect and pHpzc on removal methylene blue adsorption

The effect of pH mainly depends on the ions available in the solution and the electrostatic interaction of the ions with the surface of the adsorbent influencing the binding sites of the adsorbents [51]. The point of zero charge (pH_{PZC}) is the solution pH in which the material has zero surface charge. In this study, the adsorbent presented pH_{PZC} = 5.9 (Fig. 2b). This indicates that at $pH > pH_{PZC}$ the adsorbent is in its ionic (negatively charged) form and, therefore, there is a better attraction for species with positive charges, for example MB. However, when $pH < pH_{PZC}$ the adsorbent is positively loaded, resulting in low affinity amid the adsorbent and the MB.

The influence of initial pH on MB removal was assessed varying the pH from 2 to 10 (Fig. 2c). A decrease in the adsorption rate was observed at lower pHs. This was because, at acidic pHs, ionic repulsion happens between the positively loaded adsorbent surface by H^+ ions and the MB [52]. However, when the pH of the solution is neutral or alkaline, the MB removal rate is higher. As the pH increases, the adsorbent

surface is deprotonated and negatively charged, resulting in electrostatic adsorption between the adsorbent and the MB, thus increasing the adsorption effect. [53]. Therefore, the chosen pH was 10 for a dosage of 0.8 $g.L^{-1}$ of adsorbent.

3.4 Adsorption kinetic profiles

Figure 3a presents the effect of contact time on the adsorption capacity (q_t) of MB. The adsorption efficiency augmented fast in the initial minutes, starting to increase more slowly until reaching equilibrium before 60 min for practically all concentrations. This behavior that presents a fast initial rate followed by a slower rate is that in the initial stage there are more active sites available on the adsorbent surface, so the adsorption was easy and fast. After a period of time, the adsorption sites reduce and the MB concentration diminished. Then the adsorption efficiency gradually decline and dynamic equilibrium is reached [30]. Once the initial concentration augmented from 50 to 200 $mg.L^{-1}$, the adsorption capacity increased from 44.50 to 155.11 $mg.g^{-1}$. The higher initial adsorbate concentration increases the effective area of contact with the adsorbent and provides the driving force required to reduce the mass transfer resistance, which increases the adsorption capacity [54]. Similar behavior was reported by Neupane et al. (2014), on the adsorption of crystal violet powder from pineapple leaves.

To better understand and describe the adsorption of MB in the prepared leaf powder, the aforementioned kinetic models were used. The estimated parameters of each model are shown in Table 1. The choice of the best model was based on the statistical indicators and the physical meaning of the parameters. The highest correlation coefficient (R^2 = 0.9907) and the lowest mean relative error (ARE = 2.72%) indicate that the Pseudo-second order model fitted better to the kinetic experimental data. In the literature, it is possible to find a multitude of works that present a good kinetic fit to this model, where many indicate that the material surface tends to be more heterogeneous [12, 55, 56]. Furthermore, the results show good agreement between the experimental data (q_t) and the calculated values (q_t) from the kinetic adjustment of MB by the pseudo-second-order model, with a maximum capacity of 150.96 $mg.g^{-1}$ at the highest concentration studied at 200 $mg.L^{-1}$. The Elovich model also presented with statistical indicators, being able to be used to represent the kinetic data. On the other hand, the pseudo-first order and Avrami models obtained the least statistical indices.

3.5 Equilibrium isotherms

The adsorption equilibrium isotherms were obtained at four temperatures (298-318K) as shown in Fig. 3b. Adsorption isotherms can be classified as L2 [57], as a plateau was formed, demonstrating the overload of adsorption sites. Instead, the adsorption capacity decreased with temperature increasing, reaching the maximum values (q_e) at 298 K. For this same interval, the capacity decreased from 200 $mg.g^{-1}$ (298 K) to 174 mg g^{-1} (328 K). Evidently, the adsorption capacity declines with the intensification in temperature, indicating an exothermic process. A similar trend was also found by other authors for MB removal [1, 52, 58–60].

Table 1
Kinetic parameters on the adsorptive removal of MB.

Models	C_0 (mg L^{-1})			
	50	100	150	200
Pseudo-first order				
q_1 (mg.g^{-1})	40.8833	94.1073	125.1999	141.5128
k_1 (min^{-1})	0.2115	0.1805	0.1444	0.1649
R^2	0.9715	0.9722	0.9590	0.9669
Adj. R^2	0.9250	0.9269	0.8930	0.9131
ARE (%)	5.2774	5.9366	7.3909	6.1702
MSE (mg.g^{-1})²	6.1029	31.8172	84.2856	86.7177
Pseudo-second order				
q_2 (mg.g^{-1})	43.1257	99.9745	133.8046	151.0029
k_2 (g.mg^{-1}.min^{-1})	0.0086	0.0030	0.0017	0.0018
R^2	0.9947	0.9975	0.9913	0.9949
Adj. R^2	0.9860	0.9934	0.9768	0.9864
ARE (%)	2.2353	1.7596	3.0541	2.4209
MSE (mg.g^{-1})²	1.1256	2.8309	17.9925	13.3287
Elovich				
a (mg.g^{-1}.min^{-1})	2648.8677	1849.3463	729.0919	1286.1702
b (g.mg^{-1})	0.2652	0.1019	0.0664	0.0617
R^2	0.9933	0.9889	0.9834	0.9922
Adj. R^2	0.9822	0.9706	0.9562	0.9793
ARE (%)	2.4542	3.2859	4.2631	3.0031
MSE (mg.g^{-1})²	1.4310	12.6897	34.0450	20.4252
Avrami				

Models	C_0 (mg L^{-1})			
	50	**100**	**150**	**200**
q_{av} (mg.g^{-1})	40.8933	94.03	125.06	141.44
k_{av} (min^{-1})	0.4574	0.4281	0.3848	0.4084
n_{av}	0.4574	0.4281	0.3778	0.4084
R^2	0.9715	0.9711	0.9564	0.9659
R^2_{adj}	0.9620	0.9614	0.9419	0.9545
ARE (%)	4.7105	5.2809	6.5832	6.3997
MSE (mg.g^{-1})²	4.7532	24.7843	65.5745	67.4978
q_e (exp) (mg.g^{-1})	**44.4964**	**99.4976**	**131.58**	**155.11**

Table 2
Adsorption isotherm model parameter analysis.

Temperature (K)				
Model	**298**	**308**	**318**	**328**
Langmuir				
q_{mL} ($mg.g^{-1}$)	225.8032	219.0591	209.6389	192.8882
k_L ($L.mg^{-1}$)	0.0266	0.0249	0.0235	0.0233
R^2	0.9959	0.9944	0.9933	0.9957
R^2_{adj}	0.9938	0.9916	0.9899	0.9936
ARE (%)	5.0888	5.8622	6.2578	4.7974
MSR $(mg.g^{-1})^2$	26.3937	33.3994	36.5577	19.7367
Freundlich				
k_F $((mg.g^{-1})(mg.L^{-1})^{-1/nF})$	86.2242	82.9068	78.9530	73.4421
$1/n_F$ (dimensionless)	0.1136	0.1136	0.1136	0.1136
R^2	0.7580	0.7576	0.7618	0.7760
R^2_{adj}	0.6369	0.6364	0.6427	0.6640
ARE (%)	38.1269	37.5064	36.0013	33.3752
MSR $(mg.g^{-1})^2$	1555.2233	1447.8469	1291.4651	1030.9600
Dubinin-Radushkevich				
q_{mDR} ($mg.g^{-1}$)	177.7004	170.3421	161.8381	148.6726
$\beta x10^5$ ($kJ^2.mol^{-1}$)	6.5791	6.2454	6.2444	5.7777
R^2	0.9322	0.9363	0.9305	0.9288
R^2_{adj}	0.8983	0.9045	0.8958	0.8931
ARE (%)	19.6723	17.9983	17.7502	17.2337
MSR $(mg.g^{-1})^2$	435.6814	380.4222	376.5513	327.8553
Tempkin				

Temperature (K)				
a ($mg.g^{-1}$)	52.9117	55.7229	59.8590	67.6834
b ($L.mg^{-1}$)	0.2810	0.2560	0.2406	0.2447
R^2	0.9657	0.9694	0.9757	0.9771
R^2_{adj}	0.8870	0.8939	0.8842	0.8813
ARE (%)	7.4658	7.6116	6.5362	6.0065
MSR $(mg.g^{-1})^2$	112.9783	93.2060	66.1828	51.1229

To better understand the adsorption process, the isothermal data were fitted to the Langmuir, Freundlich, Dubinin-Radushkevich, and Tempkin models (Table 3). To determine the best model, the statistical coefficients were analyzed. In terms of best to smallest statistical fit, the Langmuir model was the one that best fitted the experimental data, followed by the Tempkin, Dubinin-Radushkevich, and Freundlich models. The Langmuir monolayer model showed high values of correlation coefficient ($R^2 > 0.9933$), and adjusted coefficient of determination ($R^2_{adj} > 0.9899$) and lower values of ARE (< 6.2578%) and MSR (< 36.5577 $mg.g^{-1}$). On the other hand, the Freundlich model presented the lowest values of ($R^2 < 0.776$), and ($R^2_{adj} < 0.664$) and the highest values of ARE (> 33.3752%) and MSR (> 1030.960 $mg.g^{-1}$). In addition, the Langmuir model presented capacity values close to those obtained experimentally, decreasing the capacity from 225.8032 to 192.8882 $mg.g^{-1}$, with the increase of the temperature in the system (298 K to 328 K). This model indicates that the accommodation of molecules on the surface of the adsorbate occurs through the formation of monolayers, distributed on surfaces with homogeneous sites[61].

Table S2 shows the comparison of the maximum adsorption capacity of the MB dye in several adsorbents present in the literature. The foliar powder of the species *Sansevieria trifasciata* showed an adsorption capacity close to that found in the literature. However, it is worth mentioning the great advantage of this material, because it does not present any chemical modification, and it comes from residual biomass.

3.6 Thermodynamic parameters

The thermodynamics parameters, standard change Gibbs (ΔG^0, $kJ.mol^{-1}$), standard change enthalpy (ΔH^0, kJ mol^{-1}), and change standard entropy ΔS^0 ($kJ.mol^{-1}.K^{-1}$) were estimated from the equilibrium constants, and are displayed in Table S3. The values of ΔG^0 and $\Delta H^0 < 0$ show that the adsorption process is spontaneous and exothermic, respectively (Mohammadi; Abdolvand, 2021). The magnitude of the ΔH^0 value confirms the physisorption nature of the adsorption process (Pal et al., 2018). Furthermore, the positive values of ΔS^0 indicate increased randomness in the solid-liquid interphase throughout the adsorption period. (Kundu, Mondal, 2019).

3.7 Simulation of dyeing effluent treatment

The leaf powder was analyzed in a synthetic mixture containing various dyes and salts (Table 1). In this study, 0.8 $g.L^{-1}$ of adsorbent was added to 50 mL of effluent under stirring at 150 rpm for 2 h at room temperature (298 K). The visible spectra of the effluent before and after the treatments are shown in Fig. 4. It is possible to verify that the spectra of the effluent after the treatment was strongly amortized, indicating an efficient color removal. The percentage of color removal from the simulated effluent was 51.5%. Therefore, it is possible to conclude that the foliar residues of the species studied are a low-cost material with great potential to be applied in the treatment of textile dye effluents.

3.8 Fixed bed adsorption performance

Seeking to analyze the behavior of the adsorbent in a fixed bed column, aiming its possible future application in real scale, continuous experiments were carried out. The results are shown in Fig. 10. The column can operate for 1430, 1130, and 525 min for concentrations of 100, 200, and 500 $mg.L^{-1}$, respectively, without adsorbent regeneration. In this case, until the break-up time, the fluid exiting the column had a clear color. After the break-up time, the color began to appear, until reaching equilibrium, in the region of the exhaustion time for each concentration. The relation between the increase of the breakthrough time with the diminishing of the initial concentration is related to the mass transfer effects on the fixed bed. Lower initial concentrations tend to generate lower driving force and low mass transfer rate, thus, requiring more time to achieve the equilibrium and leading to higher adsorption capacity [62].

The parameters for the dynamic models are showed in Table 3. The good fit with the experimental data is confimed by R^2 of > 0.99829 and MSE of $< 0.0106 \times 10^{-5}$. Thomas model forecast the adsorption capacity with an accuracy higher than 0.99829%. Also, the Yoon–Nelson model achieved an accuracy higher than 0.9983 regarding the τ. This shows that models can be used to describe the fixed bed adsorption of MB on the adsorbent. These results revealed that the waste from *Sansevieria trifasciata* is auspicious to treat dyed effluents in continuous operation mode.

Table 3
Parameters for the dynamic models.

Models	Initial concentration ($mg.L^{-1}$)		
	100	**200**	**500**
Thomas			
k_{th} ($mL.mg^{-1}.min^{-1}$)	0.10918	0.0603	0.0604
q_{eq} ($mg.g^{-1}$)	61.10165	188.3176	325.7264
$q_{eq.exp}$ ($mg.g^{-1}$)	60.48261	187.0147	322.6535
R^2	0.99829	0.9995	0.9992
MSE	0.00026	0.0001	0.0002
Yoon-Nelson			
k_{yn} (min^{-1})	0.0109	0.0121	0.0302
τ (min)	1222.0329	941.5880	434.3019
τ_{exp} (min)	830.0000	780	380
R^2	0.9983	0.9995	0.9992
MSE	0.0106	0.0003	0.0007

4. Conclusions

The prepared leaf powder of the ornamental species *Sansevieria trifasciata* proved to be efficient both for the removal of methylene blue dye and for a synthetic mixture containing several industrial dyes, for a dosage of 0.8 $g.L^{-1}$, and alkaline pH conditions. The kinetic curves showed a good statistical fit to the pseudo-second order model, with equilibrium quickly reached before 60 min of operation, regardless of concentration. Langmuir model suitable fitted the isothermal data presenting a maximum adsorption capacity of 225.8 $mg.g^{-1}$, at the lowest temperature studied (298 K). From the thermodynamic point of view, the process was spontaneous, favorable, and exothermic in nature (ΔH^0 = -5.06 $kJ.mol^{-1}$). The adsorbent showed a removal percentage of 51.5% for the synthetic effluent. Regarding the adsorption in fixed bed, breakthrough times were 1430, 1130, and 525 min for concentrations of 100, 200, and 500 $mg.L^{-1}$, respectively. Both dynamic models (Thomas and Yoon–Nelson) described the fixed bed adsorption of MB on the adsorbent. Therefore, the application of the residual leaves of *Sansevieria trifasciata* in its natura form is efficient for the dye removal, presenting a low cost of obtaining and

operating. Besides, it was observed fast kinetics and high removal at the pH of original solution and at room temperature.

References

1. A. Mohammadi, H. Abdolvand, A.P. Isfahani, Alginate beads impregnated with sulfonate containing calix[4]arene-intercalated layered double hydroxides: In situ preparation, characterization and methylene blue adsorption studies, Int. J. Biol. Macromol. 146 (2020) 89–98. https://doi.org/10.1016/j.ijbiomac.2019.12.229.
2. S.N. Jain, S.R. Tamboli, D.S. Sutar, S.R. Jadhav, J. V. Marathe, A.A. Shaikh, A.A. Prajapati, Batch and continuous studies for adsorption of anionic dye onto waste tea residue: Kinetic, equilibrium, breakthrough and reusability studies, J. Clean. Prod. 252 (2020) 119778. https://doi.org/10.1016/j.jclepro.2019.119778.
3. A. Kundu, A. Mondal, Kinetics, isotherm, and thermodynamic studies of methylene blue selective adsorption and photocatalysis of malachite green from aqueous solution using layered Na-intercalated Cu-doped Titania, Appl. Clay Sci. 183 (2019) 105323. https://doi.org/10.1016/j.clay.2019.105323.
4. L. Baloo, M.H. Isa, N. Bin Sapari, A.H. Jagaba, L.J. Wei, S. Yavari, R. Razali, R. Vasu, Adsorptive removal of methylene blue and acid orange 10 dyes from aqueous solutions using oil palm wastes-derived activated carbons, Alexandria Eng. J. 60 (2021) 5611–5629. https://doi.org/10.1016/J.AEJ.2021.04.044.
5. P.K. Malik, Dye removal from wastewater using activated carbon developed from sawdust: Adsorption equilibrium and kinetics, J. Hazard. Mater. 113 (2004) 81–88. https://doi.org/10.1016/j.jhazmat.2004.05.022.
6. K. P. Singh, D. Mohan, S. Sinha, G. S. Tondon, D. Gosh, Color Removal from Wastewater Using Low-Cost Activated Carbon Derived from Agricultural Waste Material, Ind. & Eng. Chem. Res. 42 (2003) 1965–1976. https://doi.org/10.1021/ie020800d.
7. W.J. Luo, Q. Gao, X.L. Wu, C.G. Zhou, Removal of Cationic Dye (Methylene Blue) from Aqueous Solution by Humic Acid-Modified Expanded Perlite: Experiment and Theory, Sep. Sci. Technol. 49 (2014) 2400–2411. https://doi.org/10.1080/01496395.2014.920395.
8. A.H. Jawad, A.S. Abdulhameed, Mesoporous Iraqi red kaolin clay as an efficient adsorbent for methylene blue dye: Adsorption kinetic, isotherm and mechanism study, Surfaces and Interfaces. 18 (2020) 100422. https://doi.org/10.1016/j.surfin.2019.100422.
9. T.S. Silva, L. Meili, S.H. V. Carvalho, J.I. Soletti, G.L. Dotto, E.J.S. Fonseca, Kinetics, isotherm, and thermodynamic studies of methylene blue adsorption from water by Mytella falcata waste, Environ. Sci. Pollut. Res. 24 (2017) 19927–19937. https://doi.org/10.1007/s11356-017-9645-6.
10. H. Treviño-Cordero, L.G. Juárez-Aguilar, D.I. Mendoza-Castillo, V. Hernández-Montoya, A. Bonilla-Petriciolet, M.A. Montes-Morán, Synthesis and adsorption properties of activated carbons from

biomass of Prunus domestica and Jacaranda mimosifolia for the removal of heavy metals and dyes from water, Ind. Crops Prod. 42 (2013) 315–323. https://doi.org/10.1016/j.indcrop.2012.05.029.

11. L. Wang, J. Li, Adsorption of C.I. Reactive Red 228 dye from aqueous solution by modified cellulose from flax shive: Kinetics, equilibrium, and thermodynamics, Ind. Crops Prod. 42 (2013) 153–158. https://doi.org/10.1016/j.indcrop.2012.05.031.
12. M. Rezakazemi, S. Shirazian, Lignin-chitosan blend for methylene blue removal: Adsorption modeling, J. Mol. Liq. 274 (2019) 778–791. https://doi.org/10.1016/j.molliq.2018.11.043.
13. N. Somsesta, V. Sricharoenchaikul, D. Aht-Ong, Adsorption removal of methylene blue onto activated carbon/cellulose biocomposite films: Equilibrium and kinetic studies, Mater. Chem. Phys. 240 (2020) 122221. https://doi.org/10.1016/j.matchemphys.2019.122221.
14. P. Grassi, F.C.F.C.F.C. Drumm, J. Georgin, D.S.P.D.S.P. Franco, E.L.E.L. Foletto, G.L.G.L.G.L. Dotto, S.L.S.L.S.L. Jahn, Water treatment plant sludge as iron source to catalyze a heterogeneous photo-Fenton reaction, Environ. Technol. Innov. 17 (2020) 100544. https://doi.org/10.1016/j.eti.2019.100544.
15. G.L. Dotto, G. McKay, Current scenario and challenges in adsorption for water treatment, J. Environ. Chem. Eng. 8 (2020) 103988. https://doi.org/10.1016/j.jece.2020.103988.
16. L. Meili, P.V.S. Lins, M.T. Costa, R.L. Almeida, A.K.S. Abud, J.I. Soletti, G.L. Dotto, E.H. Tanabe, L. Sellaoui, S.H.V. Carvalho, A. Erto, Adsorption of methylene blue on agroindustrial wastes: Experimental investigation and phenomenological modelling, Prog. Biophys. Mol. Biol. (2018). https://doi.org/10.1016/j.pbiomolbio.2018.07.011.
17. J. Georgin, D. Franco, F.C.F.C.F.C. Drumm, P. Grassi, M.S.M.S.M.S. Netto, D. Allasia, G.L.G.L. Dotto, Powdered biosorbent from the mandacaru cactus (cereus jamacaru) for discontinuous and continuous removal of Basic Fuchsin from aqueous solutions, Powder Technol. 364 (2020) 584–592. https://doi.org/10.1016/j.powtec.2020.01.064.
18. L. Dali Youcef, L.S. Belaroui, A. López-Galindo, Adsorption of a cationic methylene blue dye on an Algerian palygorskite, Appl. Clay Sci. 179 (2019) 105145. https://doi.org/10.1016/j.clay.2019.105145.
19. G.K. Cheruiyot, W.C. Wanyonyi, J.J. Kiplimo, E.N. Maina, Adsorption of toxic crystal violet dye using coffee husks: Equilibrium, kinetics and thermodynamics study, Sci. African. 5 (2019) 1–11. https://doi.org/10.1016/j.sciaf.2019.e00116.
20. D.S. Kharat, Preparing agricultural residue based adsorbents for removal of dyes from effluents - A review, Brazilian J. Chem. Eng. 32 (2015) 1–12. https://doi.org/10.1590/0104-6632.20150321s00003020.
21. K.A. Adegoke, O.S. Bello, Dye sequestration using agricultural wastes as adsorbents, Water Resour. Ind. 12 (2015) 8–24. https://doi.org/10.1016/j.wri.2015.09.002.
22. A.N. Módenes, C.L. Hinterholz, C. V. Neves, K. Sanderson, D.E.G. Trigueros, F.R. Espinoza-Quiñones, C.E. Borba, V. Steffen, F.B. Scheufele, A.D. Kroumov, A new alternative to use soybean hulls on the

adsorptive removal of aqueous dyestuff, Bioresour. Technol. Reports. 6 (2019) 175–182. https://doi.org/10.1016/j.biteb.2019.03.004.

23. D.S.P.D.S.P.D.S.P.D.S.P.D.S.P. Franco, E.H.E.H. Tanabe, D.A.D.A.D.A.D.A. Bertuol, G.S.G.S.G.S.G.S. Dos Reis, É.C.É.C.É.C.É.C.É.C. Lima, G.L. Dotto, Alternative treatments to improve the potential of rice husk as adsorbent for methylene blue, Water Sci. Technol. 75 (2017) 296–305. https://doi.org/10.2166/wst.2016.504.
24. M.Ş. Tanyildizi, Modeling of adsorption isotherms and kinetics of reactive dye from aqueous solution by peanut hull, Chem. Eng. J. 168 (2011) 1234–1240. https://doi.org/10.1016/j.cej.2011.02.021.
25. J. Georgin, G.L. Dotto, M.A. Mazutti, E.L. Foletto, Preparation of activated carbon from peanut shell by conventional pyrolysis and microwave irradiation-pyrolysis to remove organic dyes from aqueous solutions, J. Environ. Chem. Eng. 4 (2016) 266–275. https://doi.org/10.1016/j.jece.2015.11.018.
26. J. Georgin, F.C. Drumm, P. Grassi, D. Franco, D. Allasia, G.L. Dotto, F. Caroline, D. Patrícia, G. Dison, F. Guilherme, L. Dotto, Potential of Araucaria angustifolia bark as adsorbent to remove Gentian Violet dye from aqueous effluents, Water Sci. Technol. 78 (2018) 1693–1703. https://doi.org/10.2166/WST.2018.448.
27. P.T. Hernandes, M.L.S. Oliveira, J. Georgin, D.S.P. Franco, D. Allasia, G.L. Dotto, Adsorptive decontamination of wastewater containing methylene blue dye using golden trumpet tree bark (Handroanthus albus), Environ. Sci. Pollut. Res. (2019). https://doi.org/10.1007/s11356-019-06353-x.
28. J. Georgin, D.S.P. Franco, P. Grassi, D. Tonato, D.G.A. Piccilli, L. Meili, G.L. Dotto, Potential of Cedrella fissilis bark as an adsorbent for the removal of red 97 dye from aqueous effluents, Environ. Sci. Pollut. Res. (2019). https://doi.org/10.1007/s11356-019-05321-9.
29. M.A.M. Salleh, D.K. Mahmoud, W.A.W.A. Karim, A. Idris, Cationic and anionic dye adsorption by agricultural solid wastes: A comprehensive review, Desalination. 280 (2011) 1–13. https://doi.org/10.1016/j.desal.2011.07.019.
30. Z. Wu, W. Huang, X. Shan, Z. Li, Preparation of a porous graphene oxide/alkali lignin aerogel composite and its adsorption properties for methylene blue, Int. J. Biol. Macromol. 143 (2020) 325–333. https://doi.org/10.1016/j.ijbiomac.2019.12.017.
31. T.C. Hsu, Adsorption of an acid dye onto coal fly ash, Fuel. 87 (2008) 3040–3045. https://doi.org/10.1016/j.fuel.2008.03.026.
32. L. Bulgariu, L.B. Escudero, O.S. Bello, M. Iqbal, J. Nisar, K.A. Adegoke, F. Alakhras, M. Kornaros, I. Anastopoulos, The utilization of leaf-based adsorbents for dyes removal: A review, J. Mol. Liq. 276 (2019) 728–747. https://doi.org/10.1016/j.molliq.2018.12.001.
33. S.R. Tariq, Y. Safa, An efficient of Sansevieria trifasciata plant as biosorbent for the treatment of metal contaminated industrial effluents Farah Iqbal Abstract: Introduction : Materials and Methods :, 14 (2017).
34. B.T. Tchegnitegni, R.B. Teponno, C. Tanaka, A.F. Gabriel, L.A. Tapondjou, T. Miyamoto, Sappanin-type homoisoflavonoids from Sansevieria trifasciata Prain, Phytochem. Lett. 12 (2015) 262–266.

https://doi.org/10.1016/j.phytol.2015.04.017.

35. A.R. Cestari, E.F.S. Vieira, A.G.P. dos Santos, J.A. Mota, V.P. de Almeida, Adsorption of anionic dyes on chitosan beads. 1. The influence of the chemical structures of dyes and temperature on the adsorption kinetics, J. Colloid Interface Sci. 280 (2004) 380–386. https://doi.org/10.1016/j.jcis.2004.08.007.
36. Y.S. Ho, G. McKay, A Comparison of Chemisorption Kinetic Models Applied to Pollutant Removal on Various Sorbents, Process Saf. Environ. Prot. 76 (1998) 332–340. https://doi.org/10.1205/095758298529696.
37. S.Y. Lagergren, Zur Theorie der sogenannten Adsorption, (1898).
38. H. Freundlich, Über die Adsorption in Lösungen, Zeitschrift Für Phys. Chemie. 57U (1907). https://doi.org/10.1515/zpch-1907-5723.
39. I. Langmuir, The adsorption of gases on plane surfaces of glass, mica and platinum, Am Chem Soc. 40 (1918) 1361–1403. https://doi.org/10.1021/ja02242a004.
40. O. Redlich, D.L. Peterson, A useful adsorption isotherm, J. Phys. Chem. 63 (1959) 1024.
41. E.C. Lima, A. Hosseini-Bandegharaei, J.C. Moreno-Piraján, I. Anastopoulos, A critical review of the estimation of the thermodynamic parameters on adsorption equilibria. Wrong use of equilibrium constant in the Van't Hoof equation for calculation of thermodynamic parameters of adsorption, J. Mol. Liq. 273 (2019) 425–434. https://doi.org/10.1016/j.molliq.2018.10.048.
42. H.C. Thomas, Heterogeneous Ion Exchange in a Flowing System, J. Am. Chem. Soc. 66 (1944) 1664–1666. https://doi.org/10.1021/ja01238a017.
43. J. Georgin, D.S.P. Franco, F.C. Drumm, P. Grassi, M. Schadeck Netto, D. Allasia, G.L. Dotto, Paddle cactus (Tacinga palmadora) as potential low-cost adsorbent to treat textile effluents containing crystal violet, Chem. Eng. Commun. 207 (2020) 1368–1379. https://doi.org/10.1080/00986445.2019.1650033.
44. D.S.P. Franco, G.L. Dotto, A Short Analysis of Biosorbents and its Potential Removal Contaminants from Aqueous Media, (2020) 614–616. https://doi.org/10.33552/GJES.2020.05.000610.
45. Y.L. d. O. de O. de O. de O. Salomón, J. Georgin, D.S.P.P. Franco, M.S. Netto, P. Grassi, D.G.A.A. Piccilli, M.L.S.S. Oliveira, G.L. Dotto, Y.L. de O. Salomón, J. Georgin, D.S.P.P. Franco, M.S. Netto, P. Grassi, D.G.A.A. Piccilli, M.L.S.S. Oliveira, G.L. Dotto, Y.L. d. O. de O. de O. de O. Salomón, J. Georgin, D.S.P.P. Franco, M.S. Netto, P. Grassi, D.G.A.A. Piccilli, M.L.S.S. Oliveira, G.L. Dotto, Powdered biosorbent from pecan pericarp (Carya illinoensis) as an efficient material to uptake methyl violet 2B from effluents in batch and column operations, Adv. Powder Technol. 31 (2020) 2843–2852. https://doi.org/10.1016/j.apt.2020.05.004.
46. M. Jokar, N. Mirghaffari, M. Soleimani, M. Jabbari, Preparation and characterization of novel bio ion exchanger from medicinal herb waste (chicory) for the removal of Pb2 + and Cd2 + from aqueous solutions, J. Water Process Eng. 28 (2019) 88–99. https://doi.org/10.1016/j.jwpe.2019.01.007.
47. P. Grassi, F.C. Drumm, J. da Silveira Salla, S. Silvestri, K. da Boit Martinello, G.L. Dotto, E.L. Foletto, S.L. Jahn, Investigation of the reaction pathway for degradation of emerging contaminant in water

by photo-Fenton oxidation using fly ash as low-cost raw catalyst, Int. J. Environ. Res. 14 (2020) 427–438. https://doi.org/10.1007/s41742-020-00266-1.

48. D.S.P. Franco, J. Georgin, M.S. Netto, D. Allasia, M.L.S. Oliveira, E.L. Foletto, G.L. Dotto, Highly effective adsorption of synthetic phenol effluent by a novel activated carbon prepared from fruit wastes of the Ceiba speciosa forest species, J. Environ. Chem. Eng. 9 (2021) 105927. https://doi.org/10.1016/j.jece.2021.105927.
49. T.R. Barbosa, E.L. Foletto, G.L. Dotto, S.L. Jahn, Preparation of mesoporous geopolymer using metakaolin and rice husk ash as synthesis precursors and its use as potential adsorbent to remove organic dye from aqueous solutions, Ceram. Int. 44 (2018) 416–423. https://doi.org/10.1016/j.ceramint.2017.09.193.
50. Z. Wang, M. Gao, X. Li, J. Ning, Z. Zhou, G. Li, Efficient adsorption of methylene blue from aqueous solution by graphene oxide modified persimmon tannins, Mater. Sci. Eng. C. 108 (2020) 110196. https://doi.org/10.1016/j.msec.2019.110196.
51. S.R. Geed, K. Samal, A. Tagade, Development of adsorption-biodegradation hybrid process for removal of methylene blue from wastewater, J. Environ. Chem. Eng. 7 (2019) 103439. https://doi.org/10.1016/j.jece.2019.103439.
52. S. Liu, X. Chen, W. Ai, C. Wei, A new method to prepare mesoporous silica from coal gasification fine slag and its application in methylene blue adsorption, J. Clean. Prod. 212 (2019) 1062–1071. https://doi.org/10.1016/j.jclepro.2018.12.060.
53. J. Bu, L. Yuan, N. Zhang, D. Liu, Y. Meng, X. Peng, High-efficiency adsorption of methylene blue dye from wastewater by a thiosemicarbazide functionalized graphene oxide composite, Diam. Relat. Mater. 101 (2020) 107604. https://doi.org/10.1016/j.diamond.2019.107604.
54. M. Goswami, P. Phukan, Enhanced adsorption of cationic dyes using sulfonic acid modified activated carbon, J. Environ. Chem. Eng. 5 (2017) 3508–3517. https://doi.org/10.1016/j.jece.2017.07.016.
55. M.N. Efimov, A.A. Vasilev, D.G. Muratov, A.E. Baranchikov, G.P. Karpacheva, IR radiation assisted preparation of KOH-activated polymer-derived carbon for methylene blue adsorption, J. Environ. Chem. Eng. 7 (2019). https://doi.org/10.1016/j.jece.2019.103514.
56. C.M. Kerkhoff, K. da Boit Martinello, D.S.P.P. Franco, M.S. Netto, J. Georgin, E.L. Foletto, D.G.A.A. Piccilli, L.F.O.O. Silva, G.L. Dotto, B. Martinello, D.S.P.P. Franco, M.S. Netto, J. Georgin, E.L. Foletto, D.G.A.A. Piccilli, L.F.O.O. Silva, G.L. Dotto, K. da Boit Martinello, D.S.P.P. Franco, M.S. Netto, J. Georgin, E.L. Foletto, D.G.A.A. Piccilli, L.F.O.O. Silva, G.L. Dotto, Adsorption of ketoprofen and paracetamol and treatment of a synthetic mixture by novel porous carbon derived from Butia capitata endocarp, J. Mol. Liq. 339 (2021) 117184. https://doi.org/10.1016/j.molliq.2021.117184.
57. C.H. Giles, D. Smith, A.P. D'Silva, I.A. Easton, D. Smith, A General Treatment and Classification of the Solute Adsorption Isotherm Part I. Theoretical, J. Colloid Interface Sci. 47 (1974) 766–778. https://doi.org/10.1016/0021-9797(74)90253-7.

58. M.A. Franciski, E.C. Peres, M. Godinho, D. Perondi, E.L. Foletto, G.C. Collazzo, G.L. Dotto, Development of CO2 activated biochar from solid wastes of a beer industry and its application for methylene blue adsorption, Waste Manag. 78 (2018) 630–638. https://doi.org/10.1016/j.wasman.2018.06.040.
59. M. Gonçalves, C.S. Castro, I.K.V. Boas, F.C. Soler, E.D.C. Pinto, R.L. Lavall, W.A. Carvalho, Glycerin waste as sustainable precursor for activated carbon production: Adsorption properties and application in supercapacitors, J. Environ. Chem. Eng. 7 (2019) 103059. https://doi.org/10.1016/j.jece.2019.103059.
60. K. Pal, K. Ghorai, S. Aggrawal, T.K. Mandal, P. Mohanty, M.M. Seikh, A. Gayen, Remarkable Ti-promotion in vanadium doped anatase titania for methylene blue adsorption in aqueous medium, J. Environ. Chem. Eng. 6 (2018) 5212–5220. https://doi.org/10.1016/j.jece.2018.08.015.
61. S.S. Vedula, G.D. Yadav, Wastewater treatment containing methylene blue dye as pollutant using adsorption by chitosan lignin membrane: Development of membrane, characterization and kinetics of adsorption, J. Indian Chem. Soc. 99 (2022) 100263. https://doi.org/10.1016/j.jics.2021.100263.
62. D.S.P. Franco, J.L.S. Fagundes, J. Georgin, N.P.G. Salau, G.L. Dotto, A mass transfer study considering intraparticle diffusion and axial dispersion for fixed-bed adsorption of crystal violet on pecan pericarp (Carya illinoensis), Chem. Eng. J. 397 (2020) 125423. https://doi.org/10.1016/j.cej.2020.125423.

Figures

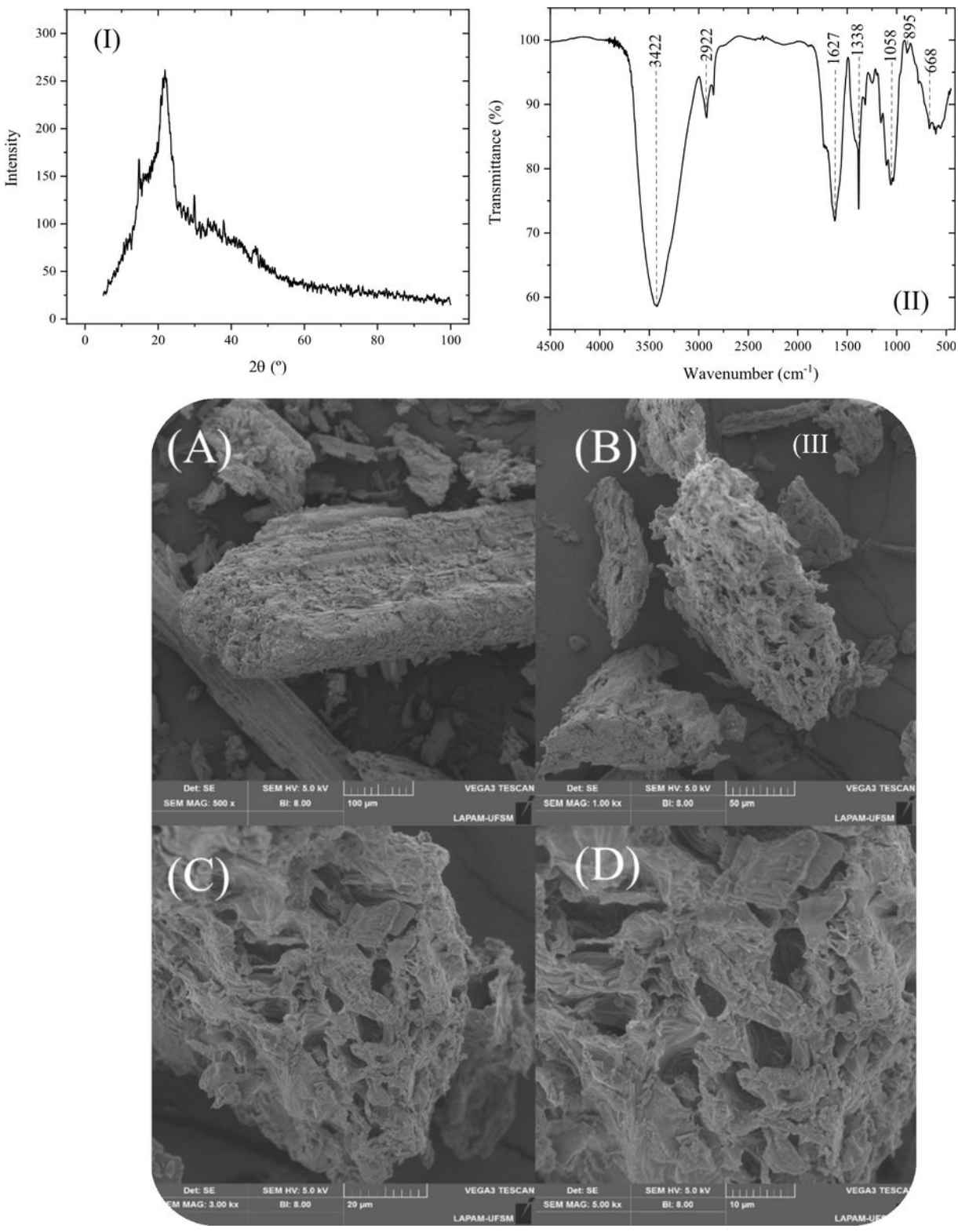

Figure 1

Characterization of *Sansevieria trifasciata*: (I) XRD; (II) FTIR; and (III) SEM images.

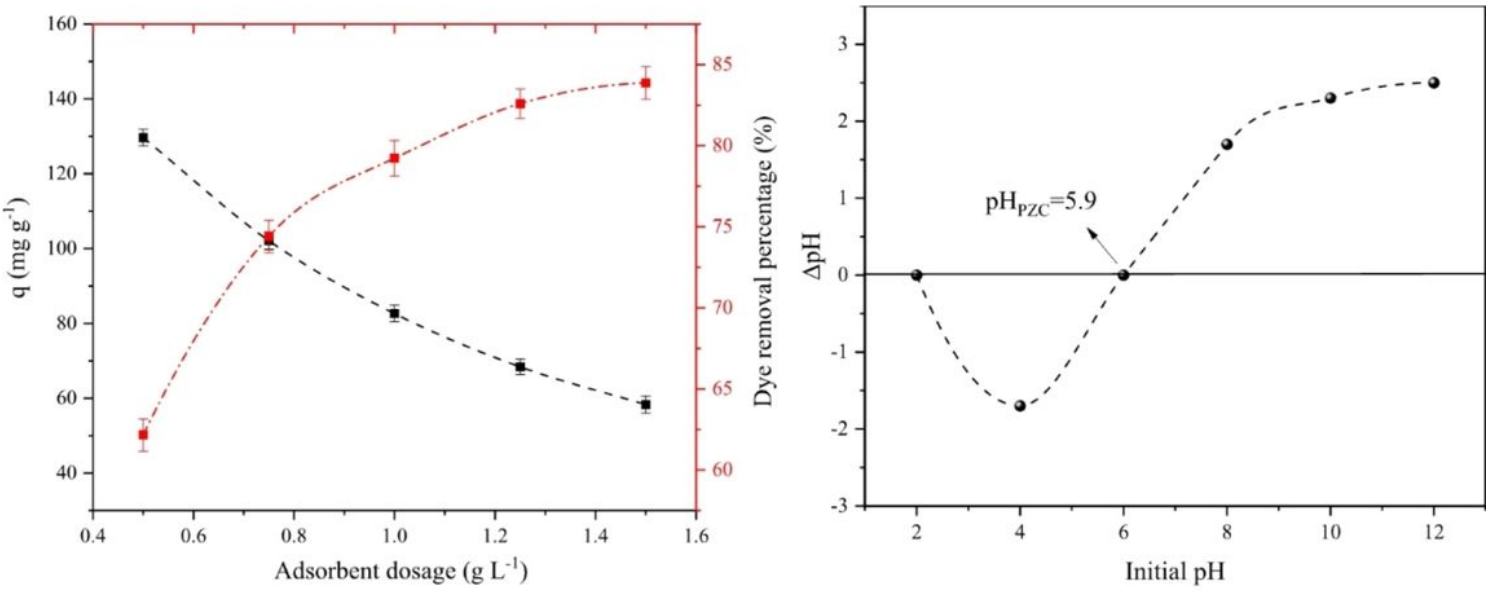

(a) (b)

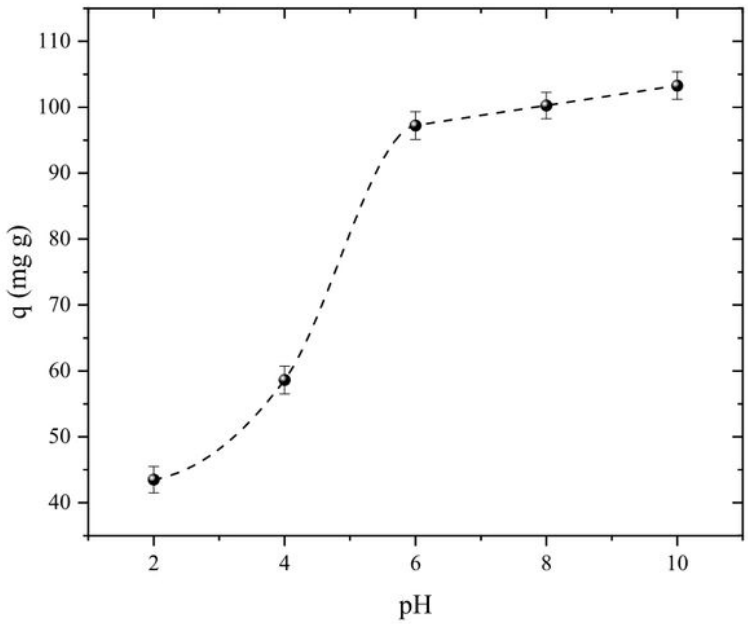

(c)

Figure 2

(a) Adsorbent dosage effect; (b) point of zero charge (pHPZC); and (c) pH effect.

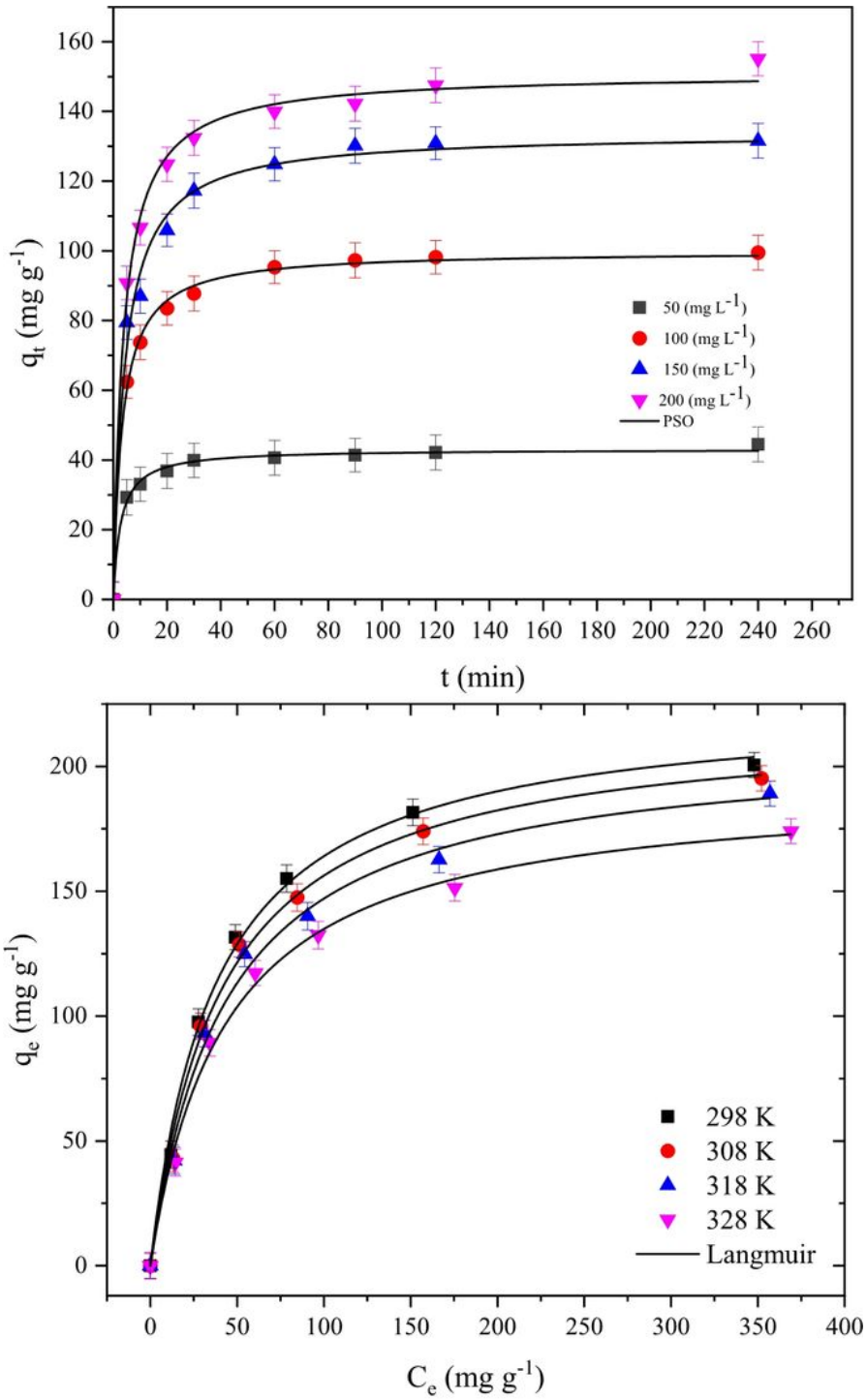

Figure 3

(a) The effect of contact time, and (b) equilibrium isotherms.

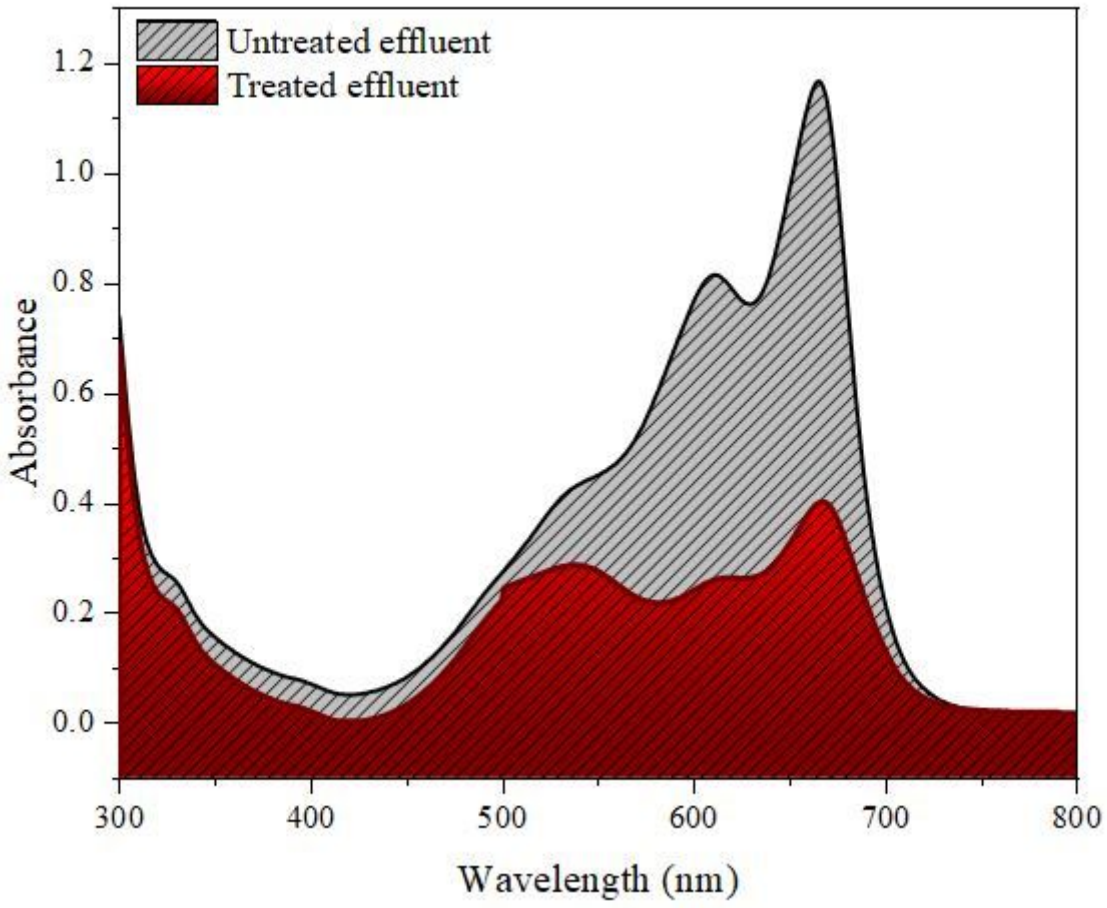

Figure 4

Spectra for the simulated effluent before and after the adsorption treatment

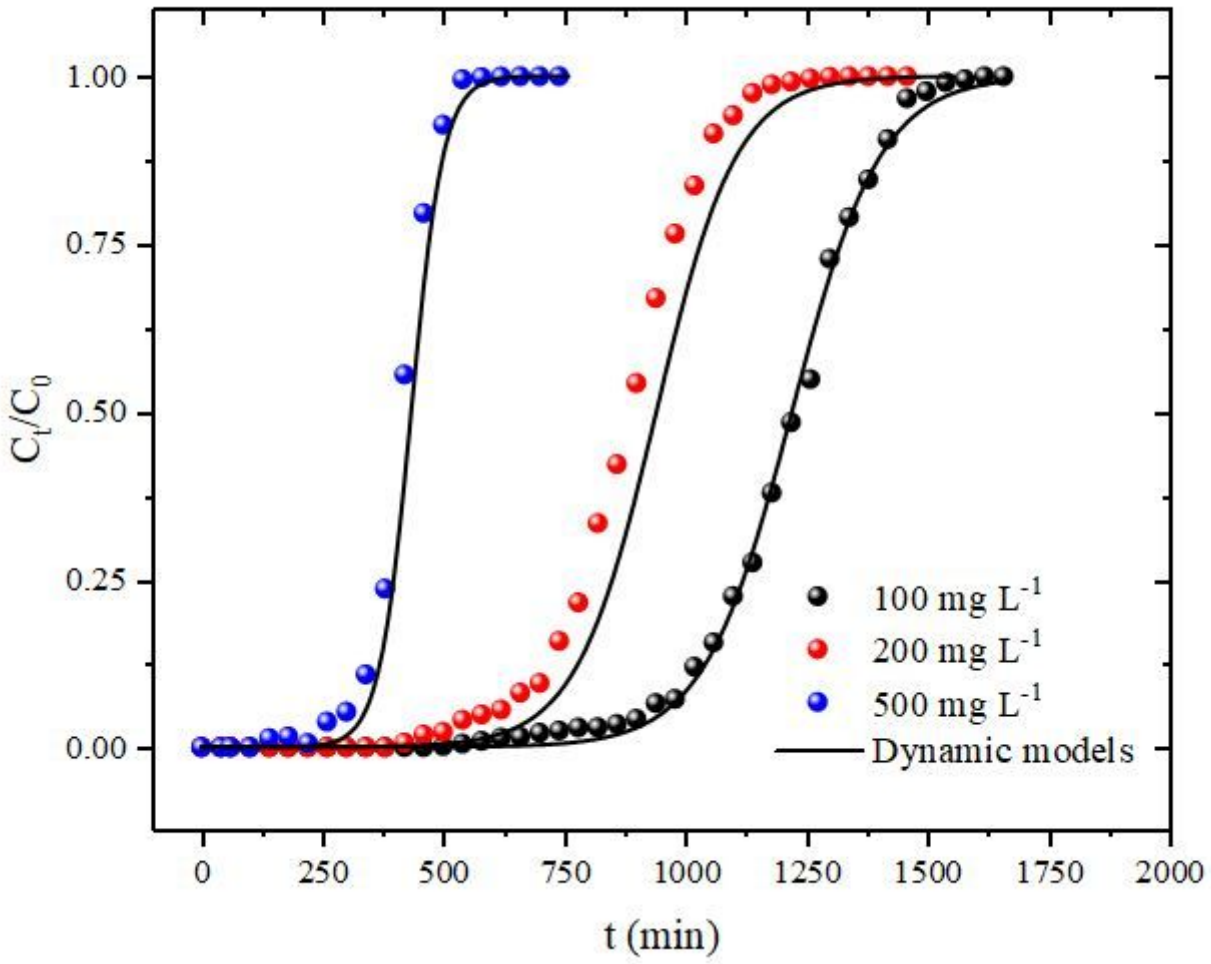

Figure 5

Measured and modeled breakthrough profiles of MB adsorption onto *Sansevieria trifasciata*

Supplementary Files

This is a list of supplementary files associated with this preprint. Click to download.

- SupplementaryMaterial.docx